EUROPEAN ORGANIZATION FOR NUCLEAR RESEARCH

PS/BD/Note 98–03
SL/BI/Note 98–027

MEASUREMENTS OF THE RELATIVE SENSITIVITIES BETWEEN SOME BEAM-LOSS MONITORS: PART II

J. Bosser and G. Ferioli

Geneva, Switzerland
25 February 1998

1 INTRODUCTION

We measured the relative sensitivity of various types of classical beam-loss monitors following on from and in the spirit of a previous work [1].

The detectors were tested in one of the SPS extraction lines. The particles passing through the line consist of 2/3 protons and 1/3 pions at 120 GeV/c. The low extracted (spill time 2.5 s) beam intensity can be adjusted. Upstream of the detectors a copper target (diameter: 7 cm, length: 50 cm) can be placed on the beam axis.

First we proceed with linearity and sensitivity measurements of various types of detectors used in counting or analog mode. Next, with a view to increasing the dynamic range we pursue our tests with a dedicated type of electronics. Finally, measurements have been made in order to determine, in the frame of our experiment, the minimum detection level of some monitors.

2 LINEARITY AND SENSITIVITY TESTS

The aim is to check for the relative sensitivity of some detectors namely:

- A scintillator with an area of 35 cm^2, coupled to a photomultiplier (PM) used in counting mode.
- Two sets of PIN diodes, PIN1 and PIN2, used also in counting mode. Each set of PIN diodes consists of two 1 cm^2 chips mounted in coincidence. It is worth remembering [1] that the natural single PIN diode counting noise is a few hundred kHz which is lowered to about 5 kHz with the help of threshold biasing voltages and to about 1 Hz by using the two diodes in coincidence.
- The 'ACEM' PS beam-loss monitor also referred to as BLPS. It consists of a photomultiplier whose active part is the thick photocathode. The PM output is connected to a resistance.
- The SPS air-filled (1 dm^3) ionization chamber: BLSPS. The chamber output signal is connected to an integrator. Its measured sensitivity is 10^{-5} C/Gy.

The mechanical set-up is shown in Fig. 1a. It is important to notice that the distance between the target output and the detectors is about 6.3 m so as to have a uniform secondary particle flux through the monitors and to avoid saturations. The detector cross-sections are shown in Fig. 1b.

2.1 Measurements

The measurements made with the above-mentioned detectors are reported in Fig. 2, while the BLPS calibration curves are given in Fig. 3. It is worth while to mention that the SPS transfer line intensity monitor has a resolution of 2×10^4 particles.

From the analysis of Fig. 2 one can see that:

a) All four detectors are quite linear. As mentioned before we managed to avoid saturation.
b) In counting mode the scintillator is more sensitive than PIN1. This results from a larger active area since when reduced to 1 cm^2 the scintillator and PIN1 counts/s are about the same. PIN2 has sensitivity a factor 4 less than PIN1; this has been checked as being an electronics issue.
c) In analog mode the PSBL is a factor 100 more sensitive than the SPSBL with, however, a large intrinsic noise level. Scaled to a cross-section of 1 cm^2 the PSBL is

700 times more sensitive than the SPSBL; this factor corresponds to the photomultiplier gain.

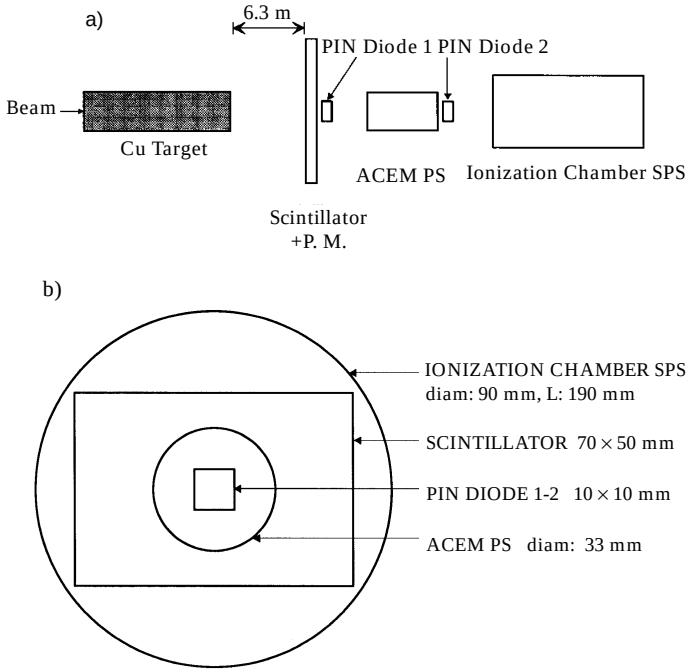

Figure 1: a) Mechanical detector set-up; b) Detector cross-sections.

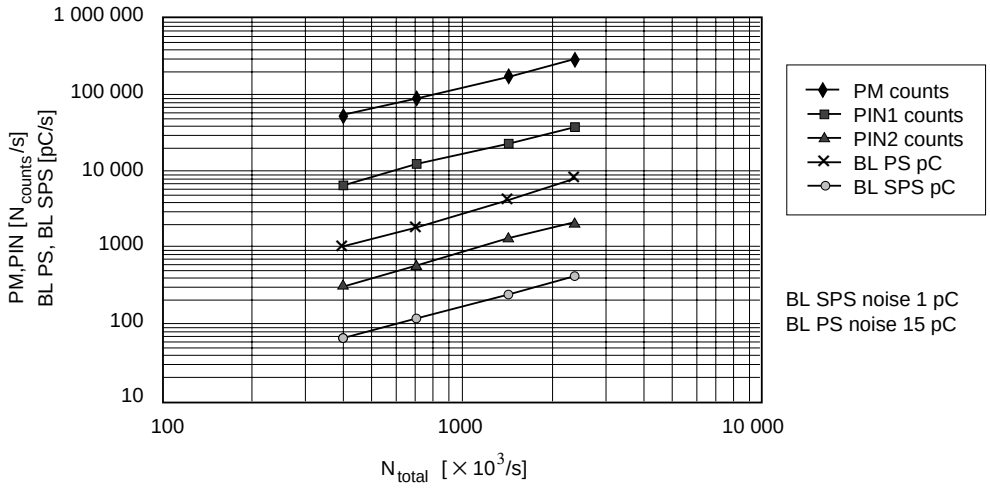

Figure 2: Detector output counts/s or pC/s versus the number of particles [10^3/s] on the target. Regression lines: PM [$N_{\mathrm{counts/s}}$] = $(2.86 + 1.278 \times 10^{-1} \times N_{\mathrm{total}}\,[10^3/\mathrm{s}]) \times 10$, PIN1 [$N_{\mathrm{counts}}$/s] = (–0.26 + $3.195 \times 10^{-3} \times N_{\mathrm{total}}\,[10^3$/s]) $\times\ 10^3$, BLPS [pC/s] = –234.52 + $18.406 \times N_{\mathrm{total}}\,[10^3$/s], BLSPS [pC/s] = –3.325 + $0.189 \times N_{\mathrm{total}}\,[10^3$/s]. High voltages [V]: PM: 1800, BLPS: 1000, BLSPS: 800.

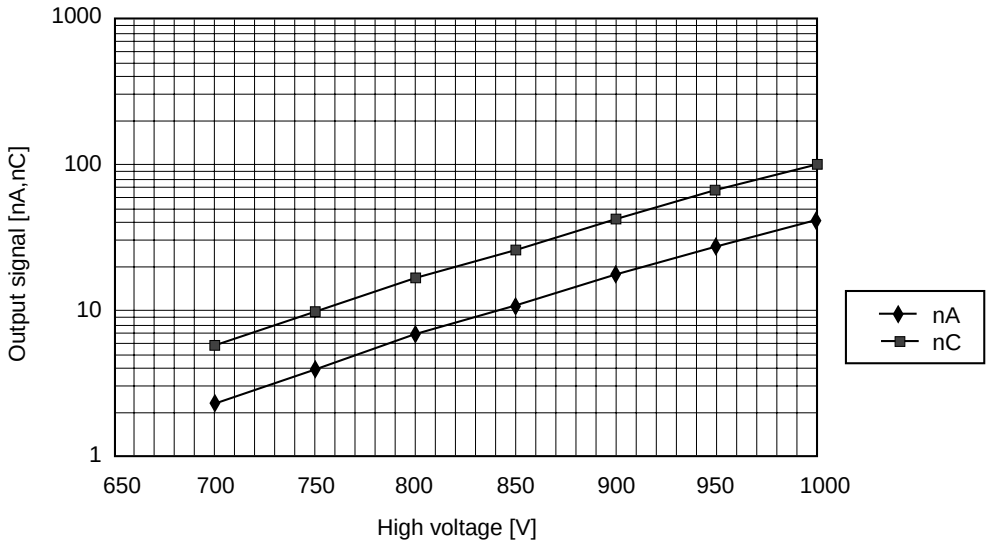

Figure 3: Calibration of the BLPS as a function of the photomultiplier (PM) high voltage [V] (horizontal axis) for a fixed number ($N_{\rm total} = 1.85 \times 10^5$ within 2.5 s) of particles on the target. The PM is loaded by a 1 MΩ resistance. Vertical axis: PM current [nA] and integrated charge [nC] within 2.5 s.

3 DYNAMIC RANGE MEASUREMENTS

As for most of the beam monitors, the loss detectors have a dynamic range which does not exceed 10^4 and is usually of the order of 10^3. The upper limit is determined by saturation or pile-up effects and the lower limit is usually fixed by the detector and electronic resolution. One can, however, foresee a wider dynamic range, of the order of 10^6, by considering, for the same detector, two separated channels: one (the 'lower range') dealing with relative losses from 1 to 10^3 and the other (the 'upper range') which covers relative losses from 10^3 to 10^6.

In this frame we developed and tested a technique based on the electronic circuits described by Figs. 4 and 5. These circuits have been used to process the 'scintillator + PM' analog output signal. One channel acts in 'counting mode' and determines, by an adequate adjustment of the discriminator voltage, the 'lower range'. The second channel, which consists of an 'integrator' with different time constants and different reset time intervals, determines the 'upper range'.

Figure 6 describes the principle of a classical charge-integrating system. It will be referred to later on.

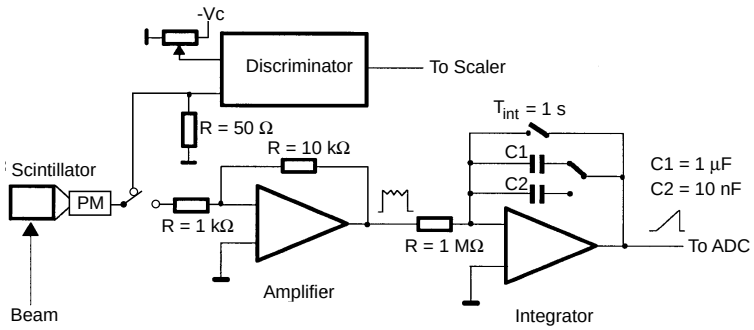

Figure 4: Electronic circuit used with the 'scintillator + PM' detector.

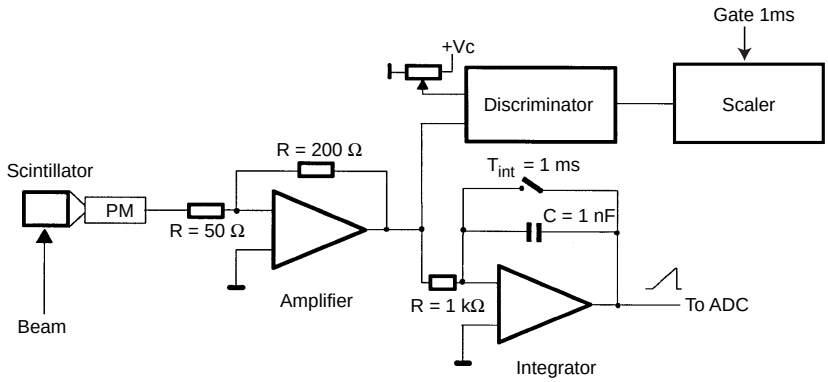

Figure 5: Identical in its principle to Fig. 4 except that the integrator uses a different time constant and is reset every millisecond. One channel operates in counting mode; it defines the lower part of the dynamic range. The second channel consists of an integrator; it aims to cope with the upper part of the dynamic range.

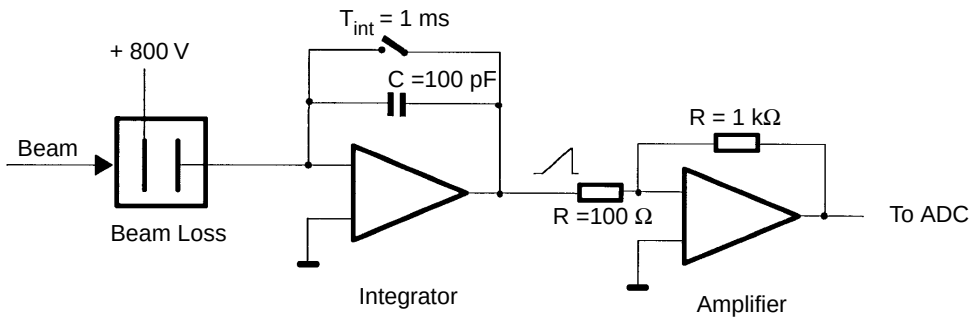

Figure 6: Principle of charge-integrating electronics.

3.1 Detectors used

One type of detector consists of a set of two PIN diodes used in coincidence as described in Section 2.

The second type of detector consists of a 'big scintillator' ($5 \times 7 \times 1\ \mathrm{cm}^3$) and of a 'small scintillator' ($3 \times 3 \times 0.5\ \mathrm{cm}^3$) coupled to a XP2020 photomultiplier.

An additional EMI photomultiplier of small dimension has also been used. The tube is plugged onto a small base powered with a 15 V DC power supply. The base itself provides all the high voltages necessary to operate the PM (anode voltage: 650 V). A cylindrical scintillator (ϕ = 2 cm, L = 10 cm) is placed on the photocathode.

The detectors are placed 1.5 or 6 m downstream of the copper target output.

3.2 Measurements

A first linearity test is made between the 'counting' and the 'integrating' modes. It concerns the large scintillator used with the circuit of Fig. 4. The results are plotted in Fig. 7. Since, for the purpose of the present measurement (aimed to check for linearity), the 'integrating' channel was intended to cope with the 'lower' range it does saturate for large particle rates on the target. Below saturation a linear and proportional response is observed. Another linearity measurement is made using the 'small scintillator' and the circuit described by Fig. 5. The results are plotted in Fig. 8. Despite some problems resulting from the primary beam instabilities a linear mapping between the two channels is observed.

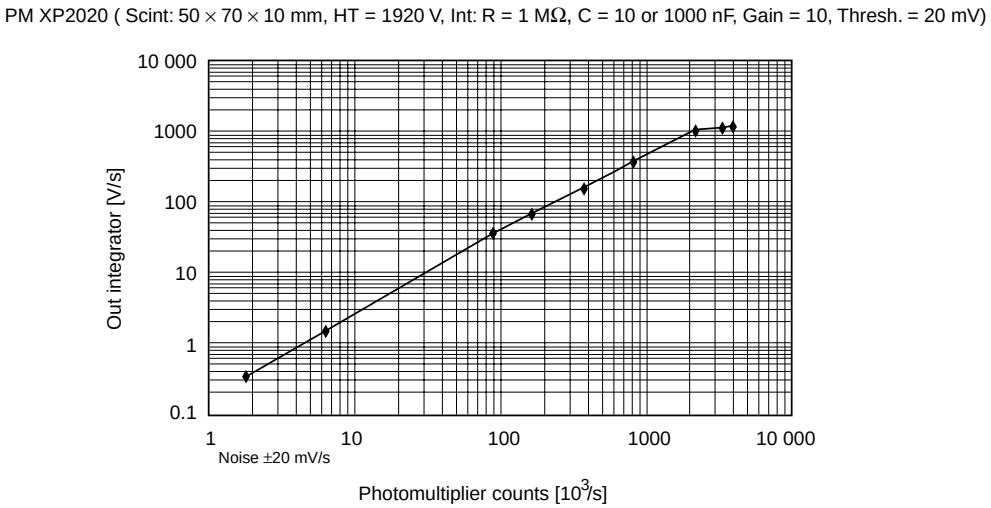

Figure 7: Comparison between counting and integrating techniques. The PM is connected to the 'big scintillator'. The PM biased at 1920 V is connected to the circuit of Fig. 4. Horizontal axis: counting rate [10^3 counts/s]. Vertical axis: integrator voltage rate [V/s]; up to 10 V/s we used a 10 nF capacitance and above a 1000 nF capacitance while keeping the same scaling on the axis.

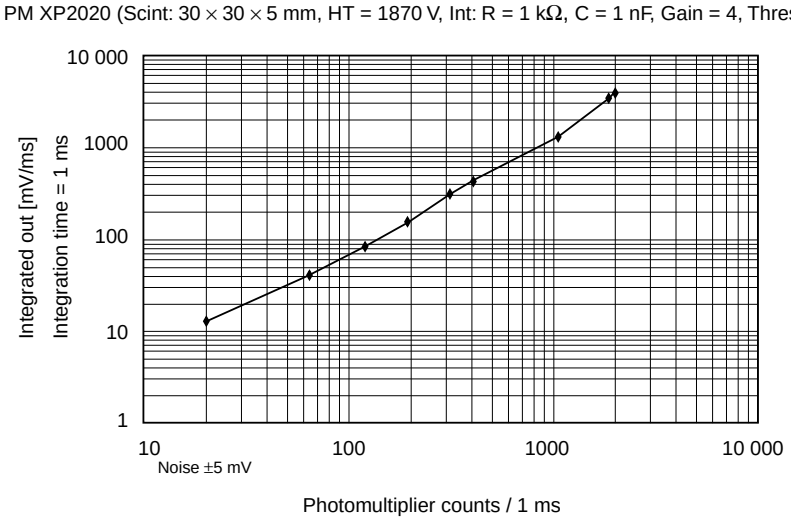

Figure 8: Comparison between counting and integrating techniques. The PM uses the 'small scintillator' and is connected to the circuit of Fig. 5. Horizontal axis: counting rate [counts/ms]. Vertical axis: integrator rate [mV/ms].

Comparative measurements involving the scintillators and the PIN diodes are summarized in Fig. 9 for large loss rates and in Fig. 10 for smaller loss rates (use of the EMI photomultiplier). From Fig. 10 we see that, as expected, the XP2020 and the EMI photomultipliers deliver the same counting rate and that the EMI tube, when used in analog mode, gives useful and workable measurements.

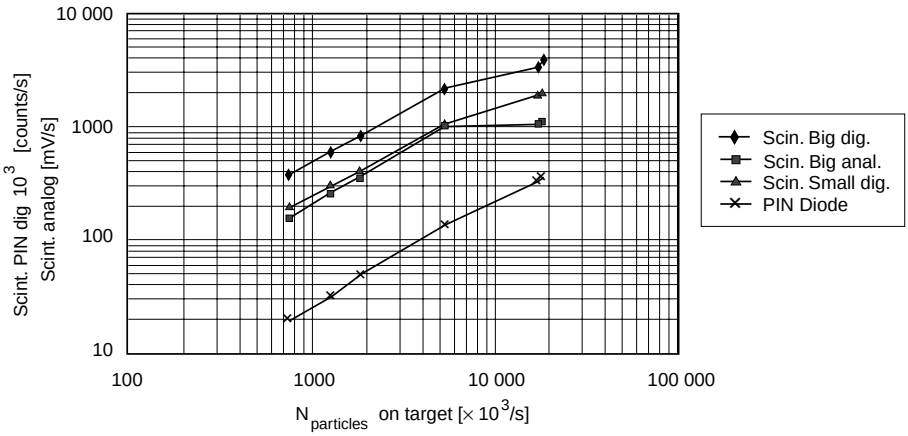

Figure 9: Comparative measurements between the scintillator, used with the XP2020 PM, and the PIN diodes. Horizontal axis: particle rate on the target [10^3/s]. Vertical axis: scintillator or PIN diode counts [10^3/s] and scintillator analog rate [mV/s]. The PM uses the circuit of Fig. 4.

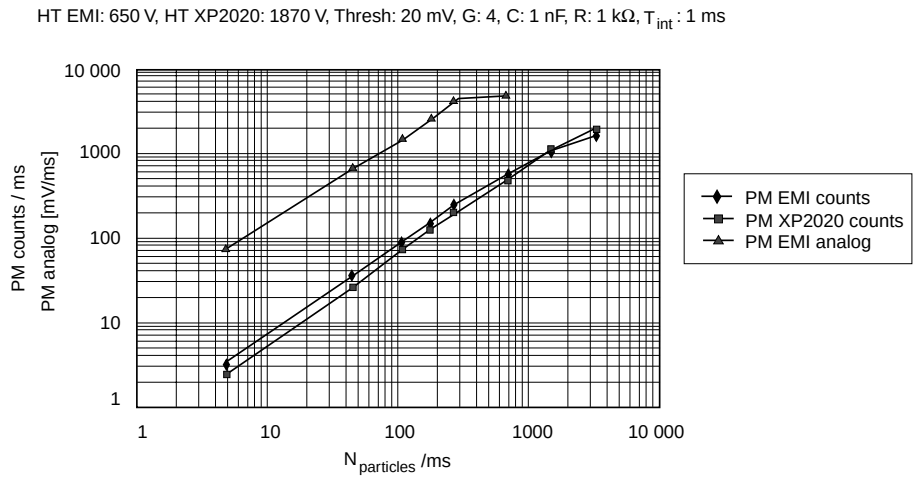

Figure 10: Comparative measurements from the scintillator, using the XP2020 or using the EMI photomultiplier. Horizontal axis: particle rate on the target/ms. Vertical axis: PM counts/ms or analog voltage rates [mV/ms]. The PMs use the circuit of Fig. 5.

3.3 Conclusions

Circuits described by Figs. 4 and 5 should allow us to cope between large and small loss rates while maintaining linear detector responses. Saturation effects in analog mode can be avoided by an appropriate choice of the electronic circuit components. It is also shown that the EMI tube with its integrated base is adequate for our purpose.

4 TESTS WITH OTHER IONIZATION MONITORS

We used two other ionization monitors coupled to the electronic circuit represented by Fig. 6.

4.1 Type of monitor

- ISR type coaxial cable. We used two cables in parallel. Each cable of 110 cm length has an outer diameter of 1.2 cm and an inner diameter of 0.3 cm so that the total active volume is $2 \times 116.6 = 233$ cm^3 filled with air at NTP. The bias voltage between the inner and the outer conductors is 800 V.
- Air-filled 'ISR' type ionization chamber. Its internal diameter is 5.5 cm and its length 25 cm so as to provide a 594 cm^3 active volume. The detector is biased at 800 V.

Both detectors were placed either parallel or orthogonal to the primary beam.

During our experiments no copper target was used so that the beam dimensions will influence our measurements. Collimators in fact control the primary beam intensity. Accurate measurements showed that (at $\pm 2 \cdot \sigma$) for a total number of particles $N_{\mathrm{p}} = 2.5 \times 10^6$, the horizontal and vertical beam widths are 13 mm and 15 mm, respectively, and that for $N_{\mathrm{p}} = 2.5 \times 10^7$, the horizontal and vertical widths are 35 mm and 15 mm, respectively.

4.2 Calibration with the SPSBL

For low intensities, i.e. $N_{\rm p} < 10^6$, we observed that the number of particles as given by the transfer line monitor and the number of counts measured by the scintillator + PMs (or PIN1, see Section 2) are about equal. Since the SPSBL has a diameter which is larger than the overall beam dimensions it is easy to proceed with a calibration of this monitor. Figure 11 gives the results. The linearity allows us to conclude that we obtain for $N_{\rm p} = 10^6$ p an integrated charge of $Q = CV = (100 \times 10^{-12} \times 8) = 0.8 \times 10^{-10}$ [C] so that in the case of $N_{\rm p} = 10^7$ p we would have a charge Q = 8 nC.

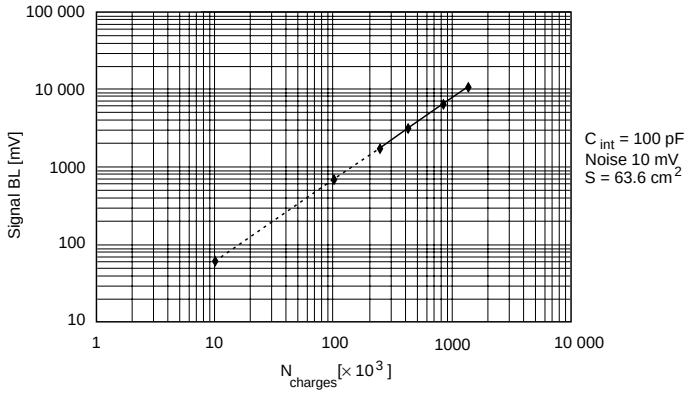

Figure 11: SPSBL calibration test. The integrating capacitance is 100 pF. Horizontal axis: total number of particle $N_{\rm p}$ $[10^3]$ passing through the chamber. Vertical axis: integrated voltage [mV].

4.3 Measurements

The measurements are given in Fig. 12. As expected the sensitivity is quite poor when the detectors are placed orthogonal to the beam. On the other hand, when placed parallel to the beam the detectors are quite sensitive.

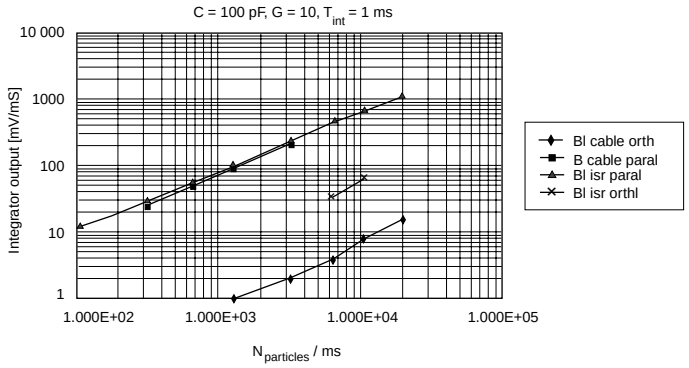

Figure 12: ISR: cable and air-filled ionization chamber detectors. Horizontal axis: number of particles on target/ms. Vertical axis: analog rates [mV/ms]. The circuit used is that described in Fig. 6.

When parallel to the beam, the cable and the ionization chamber have about the same sensitivity. These results must, however, be analysed keeping in mind the relative detector and proton beam diameters and the alignment errors between the detectors and the beam.

4.3.1 Rough estimate of the detector sensitivities

For the 'ISR cable' the ratio: length/(2 $\times$ diameter) = 110/2.4 $\cong$ 46. The signal ratio: parallel/orthogonal, for $N_{\mathrm{p}} = 3.2 \times 10^3$/ms, is about 200/2 = 100 estimated to be twice the dimension ratio. For the 'ISR ionization monitor' the ratio: length/diameter $\cong$ 25/5 = 5 while the signal ratio, at $N_{\mathrm{p}} \cong 10^4$/ms, is 600/60 = 10 which is also twice the dimension ratio. The factor 2 in favour of the parallel measurement is supposed to be due to the metallic window (which constitutes the chamber) which induces secondary particles and therefore increases the sensitivity.

4.3.2 Comparison between the 'ISR' cables and ionization monitors

Let us first consider ISR monitors placed parallel to the beam. The full beam traverses the ionization chamber over a 25 cm length. The cable itself has a length of 110 cm so one would expect the signal coming out of the cable to be a factor four larger than that of the chamber. However, one has to take into account the fact that the beam has a cross-section of 5.25 cm^2, a factor 2.5 (5.25/2.12 $\cong$ 2.5) larger than that of the cable. The cable should therefore have a sensitivity 4/2.5 = 1.6 larger than the chamber. We measured equal sensitivities (Fig. 12). This may imply that alignment issues have also to be taken into account.

We now consider 'ISR' monitors placed orthogonal to the beam. The chamber itself sees the whole beam over its 5.5 cm diameter. The cable sees part of the beam (12 mm/15 mm = 0.8) over a length of about (1.2–0.3) $\times$ 2 = 1.8 cm. Therefore the chamber should be 5.5/(1.8 $\times$ 0.8) = 4 more sensitive than the cable. We measured a factor 8 (8 = 60 mV/7.5 mV as measured on Fig. 12 for $N_{\mathrm{p}} \cong 10^4$ p/ms) in favour of the chamber. Again the factor two discrepancy may come from the fact that the cable is not accurately centred with the proton beam.

4.4 Minimum detectable amount of particles

From the above measurements we can foresee an extrapolation so we can deduce, for any of the three detectors concerned, the minimum detectable number of primary particles/ms (in the frame of the present set-up and at 120 GeV/c). The minima are given in Table 1. For the analog-type electronics, which makes use of integrators, the measured noise was $\pm$1 mV so that the extrapolated minima are taken at 5 mV. On the other hand, for the counting mode we measured practically no spurious counts.

Table 1

Detector type	Minimum (particles/ms)
EMI photomultiplier	
analog mode	1
counting mode	1
Coaxial cable	
parallel to the beam	100
orthogonal to the beam	8000
ISR ionization chamber	
parallel to the beam	70
orthogonal to the beam	1200

5 CONCLUSIONS

In the frame of our experiments both counting and analog techniques applied to various types of beam-loss monitors give valuable results. This would not be the case for bunched beams where counting techniques easily saturate.

In the present experiment the primary beam intensity could only be adjusted over a limited range. It was therefore not possible to check completely if the upper and lower ranges are complementary. However, in the intensity interval where the two ranges overlap, we got a linear correspondence between the counting and integrating modes of measurements.

The scintillator + PM detector is well-suited to our goals. Indeed the scintillator dimensions can be easily (and at low cost) adapted to the experimental contingencies as would not be the case for the other detectors, except maybe for the coaxial cable, whose dimensions cannot be easily and inexpensively arranged to fit with the experimental needs. On the other hand, the availability of integrated high-voltage ‘bases’ should avoid the distribution of the necessary PM high voltages. It must be stressed that the analog circuit’s sensitivity can easily be adapted to the loss environment through a simple change of the integrator capacitance and/or reset time.

References

[1] J. Bosser and G. Ferioli, Measurements of the relative sensitivities between some beam-loss monitors: Part I, PS/BD/Note 97–01, SL/BI/Note 97–08.